Published in Journal of Hydrology 365, issues 3-4, 275-288, 2009
which should be used for any reference to this work

Reducing the impact of a desalination plant using stochastic modeling and optimization techniques

Andres Alcolea [a,*], Philippe Renard [a], Gregoire Mariethoz [a], François Bertone [b]

[a] Centre of Hydrogeology, University of Neuchâtel, Rue Emile-Argand, 11, CP 158, CH-2009 Neuchâtel, Switzerland
[b] Egis Bceom International, 78, allée John Napier, 34965 Montpellier Cedex 2, France

S U M M A R Y

Water is critical for economic growth in coastal areas. In this context, desalination has become an increasingly important technology over the last five decades. It often has environmental side effects, especially when the input water is pumped directly from the sea via intake pipelines. However, it is generally more efficient and cheaper to desalt brackish groundwater from beach wells rather than desalting seawater. Natural attenuation is also gained and hazards due to anthropogenic pollution of seawater are reduced. In order to minimize allocation and operational costs and impacts on groundwater resources, an optimum pumping network is required. Optimization techniques are often applied to this end. Because of aquifer heterogeneity, designing the optimum pumping network demands reliable characterizations of aquifer parameters. An optimum pumping network in a coastal aquifer in Oman, where a desalination plant currently pumps brackish groundwater at a rate of 1200 m^3/h for a freshwater production of 504 m^3/h (insufficient to satisfy the growing demand in the area) was designed using stochastic inverse modeling together with optimization techniques. The Monte Carlo analysis of 200 simulations of transmissivity and storage coefficient fields conditioned to the response to stresses of tidal fluctuation and three long term pumping tests was performed. These simulations are physically plausible and fit the available data well. Simulated transmissivity fields are used to design the optimum pumping configuration required to increase the current pumping rate to 9000 m^3/h, for a freshwater production of 3346 m^3/h (more than six times larger than the existing one). For this task, new pumping wells need to be sited and their pumping rates defined. These unknowns are determined by a genetic algorithm that minimizes a function accounting for: (1) drilling, operational and maintenance costs, (2) target discharge and minimum drawdown (i.e., minimum aquifer vulnerability) and (3) technical feasibility of the solution. The performance of the optimum pumping network is compared to that of a synthetic, tradition-based hand-delineated design, where optimization is not performed. Results show that the combined use of stochastic inverse modeling and optimization techniques leads to minimum side effects (e.g., drawdowns in the area are reduced substantially) and to a significant reduction of allocation and operational costs.

Keywords: Stochastic inverse modeling, Optimization, Coastal aquifers, Groundwater, Pumping network design

Introduction

Approximately 44% of the world's population inhabits coastal areas, which represents more than the total world's population in 1950. Water is a critical factor for economic growth in these areas. Among the techniques devoted to providing freshwater in coastal areas, desalination has become increasingly important, especially during the last five decades. Actually, Delyannis (2003) found the first reference to desalination in the Bible (Exodus, 15:25; it reads of how Moses and the people of Israel came upon the waters of Merra, which were bitter: "And he cried onto the Lord. And the Lord showed him a wood and he put it into the water and the water became sweet"). Being a simple technique, the use of desalination has spread worldwide since 1950. Currently, growth is expected to be of 61% over a five-year period (from 39.9 million m^3/d at the beginning of 2006 to 64.3 million m^3/d in 2010 and 97.5 million m^3/d in 2015; GWI, 2006). However, the use of desalination is often controversial, for economic and environmental reasons. Disadvantages of desalination are the discharge of residuals, such as concentrated brine, back to the sea and an extremely high energy demand, which can add a significant contribution to greenhouse gas emissions. Often, input water is pumped directly from the sea through intake pipelines. This causes depletion of marine life (Dickie, 2007) due to impingement (i.e., death or injury due to contact with intake structures) and entrainment (i.e., marine life "sucked" by intake pipelines). Additional shortcomings are the large cost of off-shore constructions and the need for a prior filtration of seawater. These disadvantages prompted the development

* Corresponding author. Tel.: +41 32 718 2597.
E-mail addresses: andres.alcolea@unine.ch (A. Alcolea), philippe.renard@unine.ch (P. Renard), gregoire.mariethoz@unine.ch (G. Mariethoz), francois.bertone@egis.fr (F. Bertone).

of new strategies. Desalting brackish groundwater from beach wells is usually more efficient (and therefore cheaper) than desalting seawater because (1) there is less suspended matter, so the filtration processes (and consequently the cost of necessary infrastructures) are reduced and (2) the pH of brackish groundwater is about 7 (8–9 for seawater), so no neutralization or additional chemical treatment is necessary. In addition, one gains natural attenuation and hazards due to anthropogenic pollution of seawater are reduced. Nowadays, desalted brackish water represents 24% of the worldwide freshwater production (GWI, 2005).

In this context, the environmental impacts and the cost of pumping brackish groundwater can be minimized by using optimization techniques (Gorelick, 1983; Ahlfeld and Heidari, 1994; Wagner, 1995). For coastal aquifers, these techniques have been applied either to optimize freshwater pumping networks (Cheng et al., 2000; Mantoglou, 2003) or to design remediation systems (Ahlfeld and Mulligan, 2000; Abarca et al., 2006). Here, we use optimization techniques to design a pumping network for brackish groundwater. The aim is to achieve a target discharge while minimizing the environmental side effects and the demand of energy, thus minimizing the total cost of the solution. An important feature of the design is that it must be reliable regardless of the degree of aquifer heterogeneity and the corresponding uncertainty.

The need for a reliable design under uncertainty motivated the use of stochastic approaches, as opposed to single 'best' deterministic models (see reflections in Tarantola, 2005, 2006; Renard, 2007b). For coastal aquifers, Alcolea et al. (2007) integrated tidal fluctuation and injection tests in a stochastic model yielding a single 'best' estimation of the transmissivity and storage coefficient fields. Since tides can be viewed as large-scale aquifer tests, they provide large-scale information on aquifer diffusivity and connectivity patterns. Hydraulic tests improve the identification of local connectivity (Carrera and Neuman, 1986b; Meier et al., 1998; Weiss and Smith, 1998) and allow resolving diffusivity into transmissivity and storage coefficient (Carrera and Neuman, 1986a; Rotting et al., 2006). In addition, geostatistical joint interpretation of data at all boreholes provides a continuous description of the connectivity structure (i.e., of diffusivity), rather than point values of effective diffusivity at a given set of boreholes (Li et al., 2007). Also the Monte Carlo type inverse framework is used frequently for the simulation of transmissivity fields. Yet, little attention has been paid to the joint simulation of transmissivity and storage coefficient (Hendricks Franssen et al., 1999).

The objective of this paper is to demonstrate through a case study in Oman how stochastic modeling for aquifer characterization and non-linear optimization techniques can be applied to achieve a reliable design that can reduce both the environmental impacts of a desalination plant and minimize the costs of allocation and operation of the pumping system. The methodology suggested by Alcolea et al. (2007) is extended to a Monte Carlo inverse framework and is used to characterize the spatial variability of both transmissivity and storage coefficient fields from the response to tidal fluctuation and to three long term pumping tests. In that manner, 200 equally likely simulations are conditioned to available data using the regularized pilot points method (Alcolea et al., 2006a,b). The 200 simulations are physically plausible and fit the available data well. Next, transmissivity fields are used to determine the optimum pumping configuration using a genetic algorithm (Popov and Filipova, 2004; Popov, 2005) that minimizes a function accounting for: (1) the cost of allocation of wells and their maintenance, (2) the cost of electricity, which depends on drawdowns (i.e., minimum aquifer vulnerability) and (3) the technical feasibility of the solution, because only three different types of pump can be used.

The paper is organized as follows. First, the site is introduced. Second, the application of the characterization methodology is described and the results of the Monte Carlo analysis of the transmissivity and storage coefficient fields are displayed. The value of stochastic modeling is analyzed by comparing the outcomes of the conditional simulations with the 'single best' characterization obtained by conditional estimation. From that starting point, a description of the optimization procedure and the (single) optimum pumping configuration is presented. We then test the benefit of using optimization by comparing the performance of the optimum pumping configuration with the one obtained using a synthetic, tradition-based, hand-delineated pumping network (i.e., no optimization is performed for the latter case). Last, some conclusions and recommendations are summarized.

Site description and conceptual model

The study area is located on the coast of Oman. The site is occupied by a desalination plant (Fig. 1). Brackish groundwater is pumped from beach wells at a rate of 1200 m^3/h, for a freshwater production of 504 m^3/h. The purpose of the underlying study is to design a pumping network that will allow increasing the overall pumping to 9000 m^3/h. This will provide a total freshwater production of 3346 m^3/h, sufficient to satisfy the growing demand of potable water.

The aquifer is made of sub-horizontal layers of early Palaeocene–Eocene fossiliferous limestone with interbedded conglomerates laying on top of a marl deposit. Surface observations show a primary porosity in the limestone due to the lack of compaction of the sediment. Limestone often presents karstic cavities, sometimes filled with sandy silt. Thus, it is expected that most of the secondary porosity is due to karstification processes, suggesting the presence of highly diffusive conduits in the area. This hypothesis was partially confirmed by a preliminary geophysical campaign (Fig. 1). Electrical resistivity data display the presence of structures with a clear orientation toward North. However, hydraulic conductivity of these bodies could not be inferred directly from resistivity data due to the presence of brackish water, both in the highly permeable (karstified zone) and in the clayey areas.

A preliminary drilling campaign revealed that groundwater inflows towards wells are located far underneath the groundwater table. In addition, short pumping tests after drilling provided relatively high estimates of transmissivity (between 0.01 and 0.3 m^2/s) not correlated with the saturated thickness. This clearly indicates that transmissivity is governed by the karstic features in depth but not by the rock matrix. Another important observation is that groundwater is brackish all over the site. This is confirmed by the set of measurements of electrical conductivity at available boreholes, which are very similar to that of local seawater. This is explained by the extremely low amount of recharge in the area. In fact, the interface between fresh and brackish water is located several kilometers inland. These two observations show that it is reasonable to, first, neglect 3D density effects and, second, to assume that the transmissivity does not depend on head variations. This allows us to use a linearized 2D approximation of the groundwater flow equation. As a consequence, the superposition principle applies during both the characterization and optimization stages. This greatly accelerates all calculations. Yet, it is worth mentioning that the techniques used in this paper can also be applied (without too much modification) if the non linear groundwater flow equation is considered. In fact, we assume that the head variations are small relative to the aquifer thickness.

Hydraulic characterization of transmissivity and storage coefficient fields

The following is a detailed description of the characterization methodology, which includes data filtering, well testing and sto-

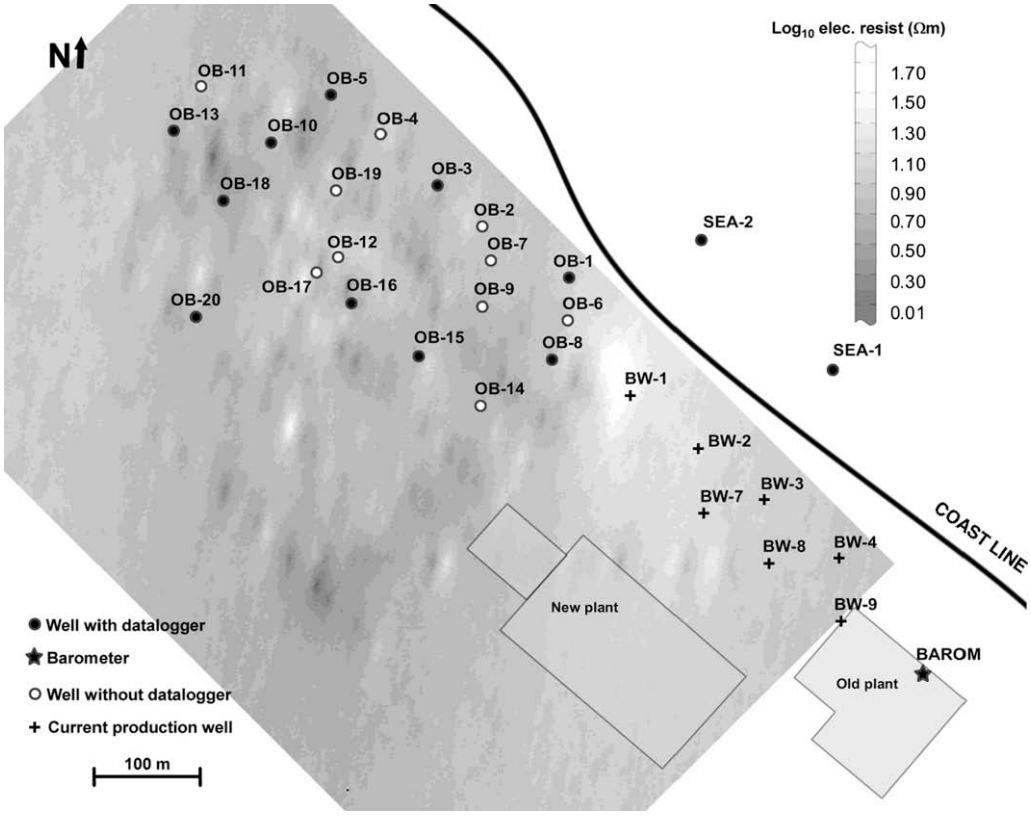

Fig. 1. Site description, observation (OB) and current production beach wells (BW). Some observation wells were automatically monitored and are depicted by black dots. Two sensors (SEA-1 and SEA-2) were located at the sea-shore for measuring the sea level fluctuation. A barometer (depicted by a star) was located at the old desalination plant. The background image depicts the ensemble mean of 100 simulations of (vertically integrated) electrical resistivity arising from a preliminary geophysical campaign.

chastic inversion. First, 200 simulations of the transmissivity and storage coefficient fields are conditioned to transmissivity, storage coefficient and head variation data (i.e., response to tidal fluctuation and to three long term pumping tests; Table 1) and their uncertainty is evaluated. The four head data sets are arranged in four independent flow problems, which are analyzed simultaneously. Second, for the sake of comparison, we also obtain a 'single best' solution by conditional estimation to the aforementioned data sets. This comparison illustrates the uncertainty overlooked by conditional estimation. Outcomes of these two sets are compared in terms of physical plausibility and fit to head variation data.

Available data

Absolute pressure (p_{abs}) was automatically recorded at the seashore (sensors SEA-1 and SEA-2) and at 10 boreholes (Fig. 1) every 30 s. Sensor SEA-2 served only as a backup in case of failure of SEA-1. First, very high frequency fluctuations of sea level due to waves and wind were filtered out as they are assumed not to propagate far away within the aquifer due to dampening effects and because the aquifer works as a high pass filter. A moving average algorithm was used to that end. Next, filtered measurements were transformed into relative pressures by subtracting the barometric pressure ($p_{rel} = p_{abs} - p_{bar}$), monitored with the same frequency at sensor BAROM. Next, relative pressures were transformed into pressure heads (p_{rel}/γ, where γ is the specific weight of groundwater). Average specific weight at available boreholes was 1021 kg/m^3, very similar to that of local seawater (i.e., the entire study area has already been intruded by seawater). Finally, heads are calculated as the sum of pressure heads and sensor elevation. This is obtained as the difference between the elevation of a reference point at the well (e.g., top of casing) and the sum of the absolute pressure and the groundwater depth (dipped manually) at a given time in absence of pumping. It is good practice to calculate the sensor elevation at different times, corresponding to low, mean and high tide to ensure unbiasedness and statistical coherency of the methodology.

Table 1
Data sets available for conditioning the stochastic model. Measurement periods of pumping tests include the recovery. Transmissivity and storage coefficient measurements arise from the (conventional) prior interpretation of hydraulic tests.

Data in response to	Monitored period (days)	Monitored wells OB – (Fig. 1)
Tidal fluctuation	7	1, 3, 5, 8, 10, 13, 15, 16, 18, 20
Pumping test at OB-6	4	1, 3, 5, 6, 8, 9, 10, 13, 14, 15, 16, 18, 20
Pumping test at OB-15	2	1, 3, 5, 8, 9, 10, 13, 14, 15, 16, 18, 20
Pumping test at OB-16	2.5	1, 3, 5, 8, 9, 10, 12, 13, 15, 16, 17, 18, 20
Transmissivity	–	All
Storage coefficient	–	1, 3, 4, 5, 9, 10, 12, 13, 14, 15, 16

Working with head fluctuations

Tidal response is expressed in terms of variation with respect to natural heads. This simplifies the boundary and initial conditions of the stochastic model, as one needs to simulate only the head variations induced by sea level fluctuations, but neither the regional flows nor the existing pumping of the desalination plant. To this end, head measurements at every borehole were corrected by subtracting their mean value. This operation simply shifts the recorded signal towards the horizontal axis (i.e., zero head fluctuation). Thus, if the signal at a well is coherent, head variations are bounded by sea level fluctuations. Calculated heads at sensors

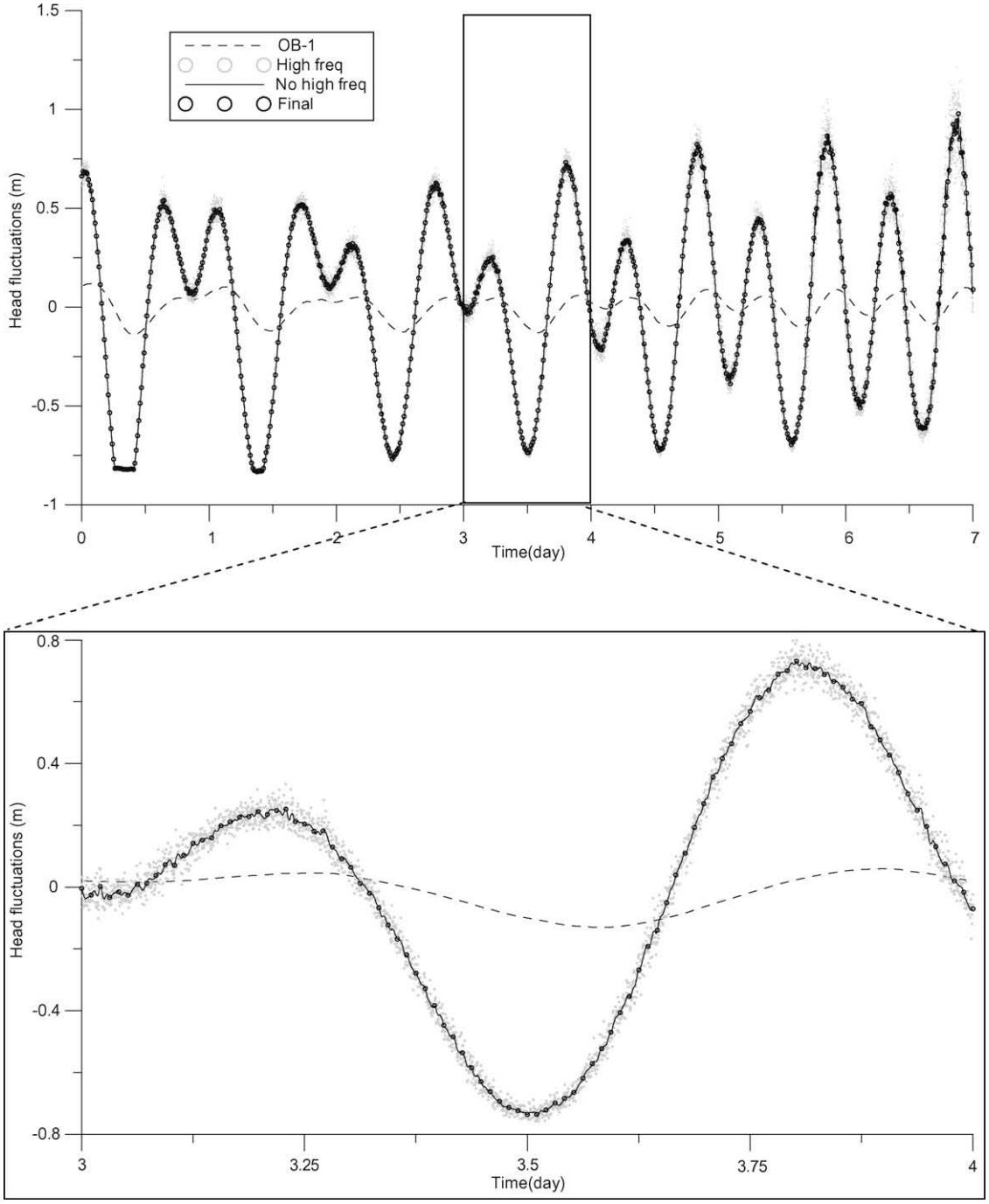

Fig. 2. Filtering the sea level fluctuation. Grey dots depict the measured sea level oscillation, containing high frequency fluctuations (i.e., due to waves and wind). The solid line is the result from a moving average filter for removing those undesired fluctuations. Finally, one measurement every 15 min is selected (black dots). Dashed line depicts the filtered head variation at observation well OB-1.

SEA-1 and OB-1 are displayed in Fig. 2. The large amount of data (~246,000 at every borehole) demands prior filtering consisting of the selection of one measurement every 15 min. This makes the data set manageable while allowing the selected measurements to capture the temporal variability of heads (Fig. 2).

Analysis of the tidal response

Analysis of the tidal response measured during two months before the start of the pumping tests allows us to estimate point values of effective diffusivity ($D_{\text{eff}} = T/S$, being T transmissivity and S storage coefficient). It is worth mentioning that diffusivity values at monitored boreholes will not be used as hard data for conditioning the stochastic model. Yet, they are valuable for checking the plausibility of the simulations. We follow roughly the steps of the tidal response method (TRM hereinafter, Jacob, 1950; Ferris, 1951; Hvorslev, 1951):

$$\Delta H^i_{well} = \Delta H^i_{sea} \exp\left(-\sqrt{\frac{\pi x^2}{t^i_0 D^i_{eff}}}\right) \quad (1)$$

where ΔH_{sea} and ΔH_{well} are the amplitudes of head fluctuations at the sea and at a well at distance x inland from the coast, respectively, and t_0 is the period of the sea level fluctuation. A multi-com-

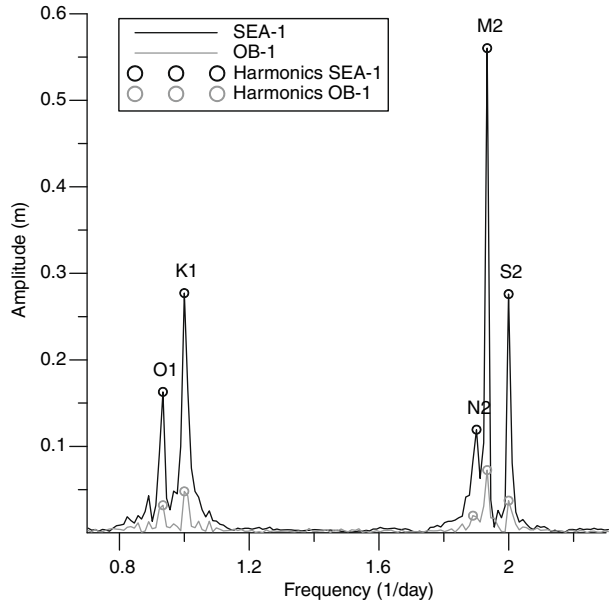

Fig. 3. Fourier spectrum of the sea level fluctuation and tidal response measured at sensors SEA-1 and OB-1, respectively. Five main harmonics are identified. From left to right, these are O1 (influence of lunar declinational diurnal wave), K1 (lunar–solar declinational diurnal), N2 (larger lunar elliptic semidiurnal), M2 (lunar semidiurnal) and S2 (solar semidiurnal). The tidal response at OB-1 is almost immediate, due to the proximity to the sea.

ponent analysis is carried out considering the main harmonics '*i*' of the sea level fluctuation. Five main harmonics were considered, with dominance of the semi-diurnal lunar principal wave (M2). Corresponding amplitudes were identified by analyzing the Fourier spectrum of the sea level fluctuation measured at sensor SEA-1 (Fig. 3). Following the same procedure, the corresponding harmonics of measured signals at monitored wells were identified. Next, effective diffusivity for a given harmonic can be obtained from Eq. (1). Table 2 summarizes the geometric average of estimated effective diffusivities (at monitored wells) using TRM, by prior interpretation of short term pumping tests and by the stochastic model. The large variability of estimated effective diffusivities confirms the highly heterogeneous character of the aquifer. A key issue in the application of TRM is the uncertainty on the knowledge of the distance between the well and the seashore. In this study, we have assumed the mean surface of seashore as boundary. Yet, the (true) contact between sea and aquifer should be accounted for. A 3D analysis of temperature profiles at the seashore may help to locate that contact.

Table 2
Summary of effective diffusivities obtained by the tidal response method, by prior (conventional) interpretation of pumping tests and by the stochastic model (average of all simulations).

	TRM	Pumping tests (HYTOOL)			Model
	D_{eff} (m^2/s)	T (m^2/s)	S (–)	D_{eff} (m^2/s)	D_{eff} (m^2/s)
OB-1	0.33	0.16	0.16	1.0	0.37
OB-2	–	0.05	–	–	–
OB-3	0.95	0.09	0.13	0.70	0.97
OB-4	–	0.33	0.08	4.07	–
OB-5	1.95	0.17	0.21	0.81	1.28
OB-6	–	0.16	–	–	–
OB-7	–	0.05	–	–	–
OB-8	3.35	0.18	–	–	2.05
OB-9	–	0.05	0.18	0.26	–
OB-10	2.12	0.28	$3.8{\cdot}10^{-4}$	737	1.36
OB-11	–	0.19	–	–	–
OB-12	–	0.05	0.10	0.52	–
OB-13	0.75	0.22	0.16	1.38	0.92
OB-14	–	0.12	0.10	1.20	–
OB-15	0.52	0.03	0.09	0.30	0.41
OB-16	0.40	0.08	0.02	3.33	0.72
OB-17	–	0.05	0.34	0.14	–
OB-18	2.33	0.30	–	–	1.58
OB-19	–	0.01	–	–	–
OB-20	4.85	0.23	–	–	1.73

Prior interpretation of pumping tests

Standard interpretation of drawdown data (i.e., assuming homogeneity) allows us to obtain a prior estimation of the hydraulic parameters characterizing the aquifer. Unfortunately, hydraulic test data are not suitable for standard analysis due to the superposition of pumping and tidal effects (Trefry and Johnston, 1998; Chen and Jiao, 1999). The difficulty consists of estimating what should have been the natural heads during the pumping periods. Several alternatives can be used for separating these effects. Alcolea et al. (2007) used kriging with external drift. TRM estimated diffusivities can also be used to this end. None of these two methodologies yielded good results for available data sets, as confirmed by cross-validation. Instead, we used records at wells not affected by pumping and signal filtering algorithms. Natural heads $h_n^i(t)$ at a well '*i*' are estimated by:

(1) Selecting the signal at another (reference) well $h^{ref}(t)$, such that, first, signals $h^{ref}(t)$ and $h^i(t)$ are highly correlated in periods not affected by pumping and, second, $h^{ref}(t)$ is not affected by pumping.
(2) Iteratively correcting the amplitude and the phase of $h^{ref}(t)$:

$$h_n^i(t) = a\left[h^{ef}(t-\tau) - \langle h_{ref}\rangle\right] + b \tag{2}$$

where τ is the time lag between both signals, $<h_{ref}>$ denotes the mean head at reference well, '*a*' is a dampening factor of amplitudes and '*b*' is a constant term that allows us to shift the heads. Parameters *a*, *b* and τ are estimated so that the differences between the reconstructed signal $h_n^i(t)$ and the measurements $h^i(t)$ are minimal in absence of pumping (i.e., we fit all measurements before and after pumping periods). Finally, drawdowns are calculated as the difference between natural heads and measured heads (See section "Available data"). The pumping tests are interpreted by conventional analysis assuming homogeneous medium. This allows us to obtain prior estimates of transmissivity and storage coefficient at monitored wells. These values will condition the stochastic model. Prior interpretation of pumping tests was carried out using the open-source software HYTOOL (Renard, 2007a), a Matlab plug-in for the interpretation of hydraulic tests. This toolbox contains analytical solutions used to describe groundwater radial flow (e.g., Jacob, Boulton, Papadopoulos-Cooper, etc.), and functions for importing, displaying and fitting a model to available data. Table 2 summarizes the estimated values of transmissivity and storage coefficient.

Measurement errors

Acquisition errors were accounted for by assigning a standard deviation of 0.005 m to tidal response data (i.e., in absence of pumping). The filtering process described in previous sections was also accounted for by assigning a larger standard deviation of 0.01 m to the estimated drawdowns during pumping periods (Table 1). Prior information arising from the conventional interpretation of pumping tests was also uncertain. Main sources of uncertainty were the conceptual model (homogeneous) and those

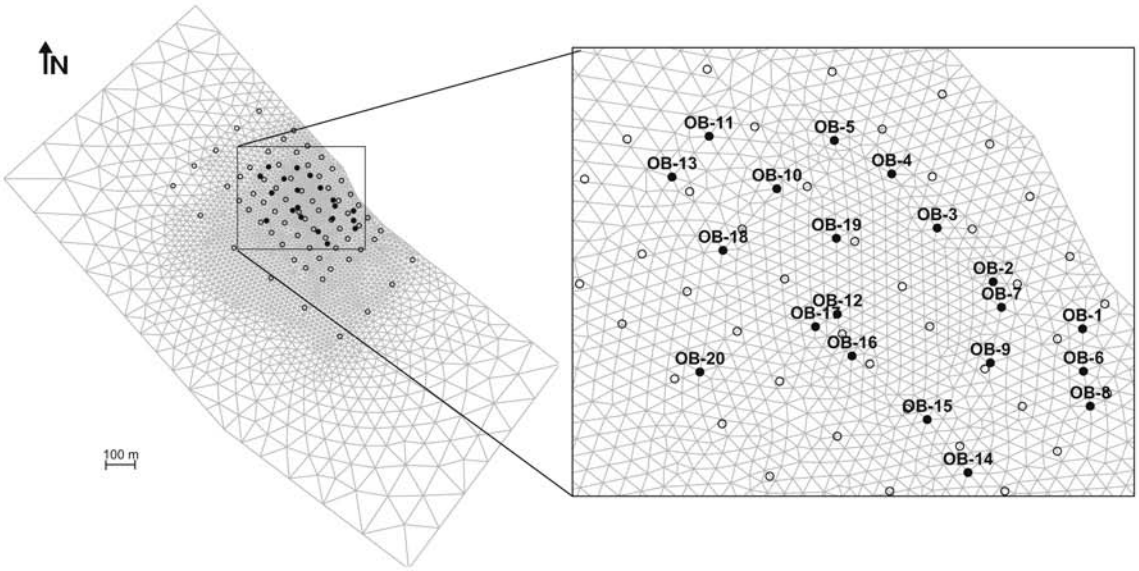

Fig. 4. Spatial discretization of the domain. The finite element mesh consists of 2585 nodes arranged in 5074 triangular elements. In the inset, existing (monitored) wells and pilot point locations are depicted by filled circles and open circles, respectively.

related to the short duration of the experiments. We assigned rather large error variances of 3 (in log scale) to the transmissivity and storage coefficient measurements used for conditioning the stochastic model (Table 2).

Spatio-temporal discretization

Two finite element codes have been used in this work: TRANSIN and GROUNDWATER. TRANSIN (Medina et al., 2000; Medina and Carrera, 2003) solves the geostatistical inverse groundwater flow and contaminant transport problem. It was used (as modified by Alcolea et al., 2006a,b) for characterizing aquifer parameters. GROUNDWATER (Cornaton, 2007) provides an exhaustive mathematical representation of physical processes governing groundwater flow and contaminant transport. It is used at the optimization stage of this work. Both TRANSIN and GROUNDWATER allow solving groundwater flow under different assumptions. In this work, the codes are used to solve the 2D groundwater flow equation assuming that T is not affected by head changes. This is equivalent to assuming a standard 2D confined aquifer hypothesis (see section "Site description and conceptual model"). The finite element mesh is designed using the code 2DUMG (Bugeda, 1990). It honors the relevant geometric features (e.g., seashore, wells, etc.) and consists of 2585 nodes, arranged in 5074 triangular elements (Fig. 4). It is refined in the vicinity of the existing observation wells and close to the seashore. The element size increases as the mesh progresses outside the area encompassing the existing wells and/or inland. Temporal behavior is modeled with a forward in time finite differences scheme. The time step is constant (15 min, equal to the measurement frequency). Simulation periods are listed in Table 1.

Boundary and initial conditions

The methodology suggested by Alcolea et al. (2007) works with head fluctuations rather than with absolute heads. In this way, one needs to simulate only head variations induced by tidal fluctuation or pumping, but neither the regional flow in the aquifer nor the existing pumping. Therefore, boundary and initial conditions are homogeneous (i.e., zero head variations and fluxes) and only the boundary conditions governing the test must be modeled explicitly by means of time functions. These are the sea level fluctuation for the tidal response and the prescribed flow rates for the pumping tests. Boundary conditions are summarized in Table 3. Likewise, areal recharge does not need to be calculated (in fact, recharge in the entire study area is negligible).

Spatial variability of unknown fields

Transmissivity and storage coefficient fields are highly heterogeneous, as revealed by the geophysical campaign (Fig. 1) and the prior estimation of effective diffusivities (Table 2). We use a geostatistical model consisting of a set of hard measurements (Table 2) and a correlation (covariance) structure arising from a preliminary study. The covariance structure is represented by a single anisotropic exponential variogram, without nugget effect and sill of 0.011 ($\log_{10}(m^2/s)$). Ranges are 600 m along the direction of larger correlation (N4W, Fig. 1) and 290 m in the orthogonal one. This covariance structure applies to both transmissivity and storage coefficient, as they are assumed to be highly correlated. The spatial variability of these parameters is characterized using the regularized pilot points method (Alcolea et al., 2006a,b). To this end, an

Table 3
Boundary conditions of the geostatistical model. PT denotes pumping test and the corresponding recovery. $\Delta H_{sea}(t)$ is depicted by dots in Fig. 2.

Boundary	Type	Problem 1. Tidal response	Problem 2. PT at OB-6	Problem 3. PT at OB-15	Problem 4. PT at OB-16
East	Prescribed flow	$Q = 0$	$Q = 0$	$Q = 0$	$Q = 0$
West	Prescribed flow	$Q = 0$	$Q = 0$	$Q = 0$	$Q = 0$
South	Prescribed flow	$Q = 0$	$Q = 0$	$Q = 0$	$Q = 0$
North, seashore	Prescribed head	$\Delta h(t) = \Delta H_{sea}(t)$	$\Delta h = 0$	$\Delta h = 0$	$\Delta h = 0$
OB-6	Prescribed flow	–	$Q = 0.1$ (m^3/s)	–	–
OB-15	Prescribed flow	–	–	$Q = 0.1$ (m^3/s)	–
OB-16	Prescribed flow	–	–	–	$Q = 0.1$ (m^3/s)

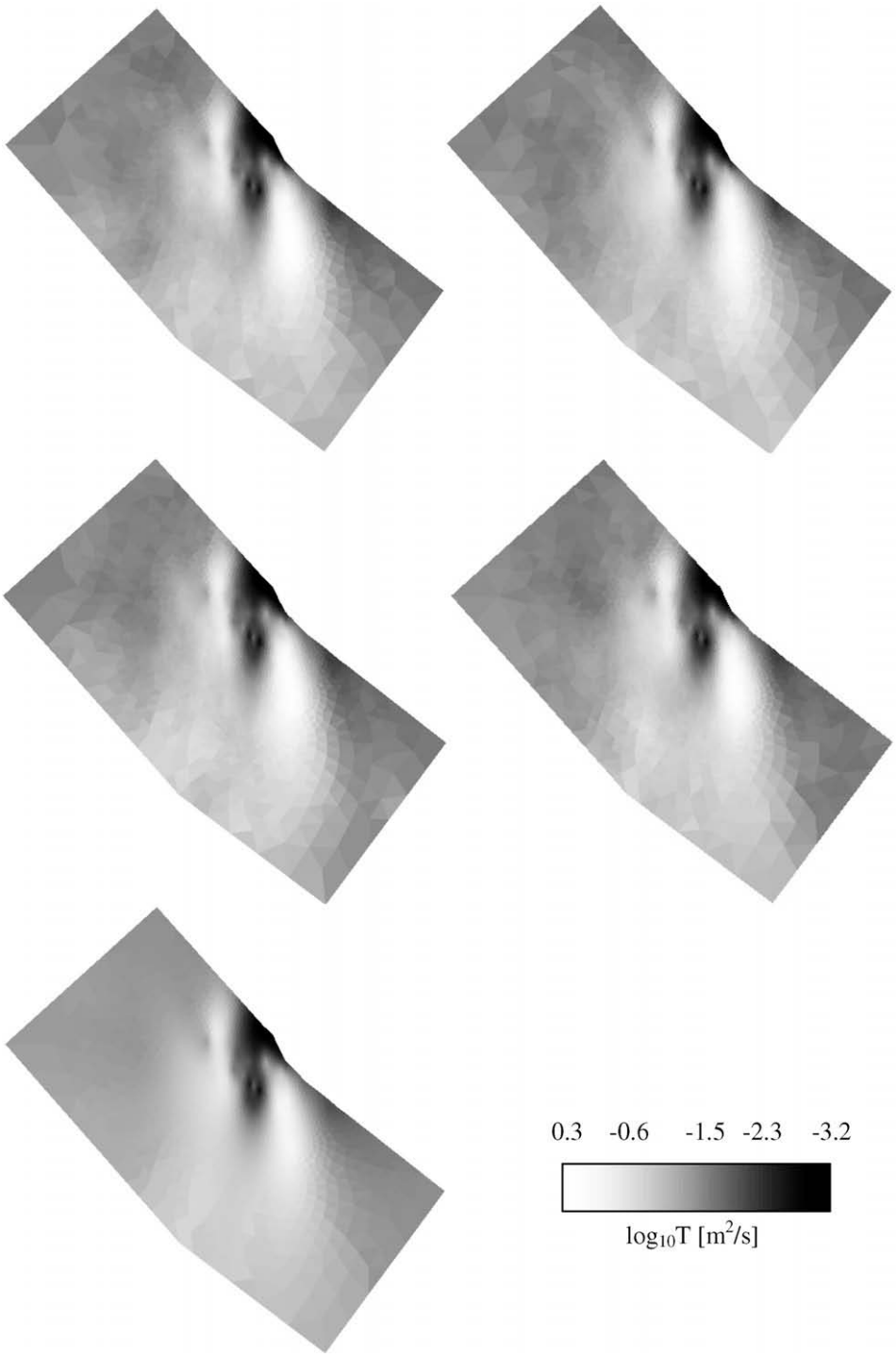

Fig. 5. Four out of two hundred conditionally simulated (above) and estimated (below) log-transmissivity fields.

unstructured network of pilot points (69 for each unknown field) has been designed. These are clustered in the zone encompassing the existing wells, where the majority of the information comes from (Fig. 4).

Results

Results are evaluated in terms of fits to available head variation measurements and plausibility of the solutions. The latter is evaluated both qualitatively (by visual comparisons with the resistivity map in Fig. 1) and quantitatively. To this end, we compare the diffusivities estimated by the model with those obtained by TRM (Table 2). Four out of two hundred simulated transmissivity and diffusivity fields (and the corresponding fields obtained by conditional estimation) are displayed in Figs. 5 and 6, respectively. Note that the unknowns are transmissivity and storage coefficient. However, observation of diffusivity ($D = T/S$) facilitates interpretation. In the 200 conditional simulations and the 'single best' conditional estimation, the monitored wells lay on a zone of medium diffusivity, connected to the sea and embedded between two parallel channels of high diffusivity. These present a clear orientation toward North and are also well connected to the sea. All character-

Fig. 6. Four out of two hundred simulated (above) and estimated (below) log-diffusivity fields, calculated as $D = T/S$.

izations reveal the presence of a low diffusivity zone close to the seashore. This can be explained by the deposition of fine, less permeable, materials along the coast line in the study area, where the marine currents are normally weak. Possibly, a Cauchy type boundary condition (i.e., leakage) at the seashore would have modeled this effect better. Yet, the fine discretization used close to the seashore (Fig. 4) helps to alleviate this problem.

Fits to head variation data are displayed in Fig. 7. They are all satisfactory, even for the simulation yielding the worst match to measured head variations. Very similar fits are obtained by conditional estimation. In spite of the smoothness of the estimated transmissivity and storage coefficient fields, conditional estimation captures the large scale patterns of heterogeneity, which are known to control groundwater flow (Alcolea et al., 2008). However, seeking a 'single best' characterization by conditional estimation is not a good option because it does not allow us to evaluate uncertainty. The quality of the fits to measured head variations is best observed in Fig. 8. There, we depict the Box and Whisker plots (boxplots hereinafter) of the averaged-in-time standardized residuals for all conditional simulations and all observation wells and problems listed in Table 1. Normalization factors are the amplitude of the tide (2.62 m) and the maximum

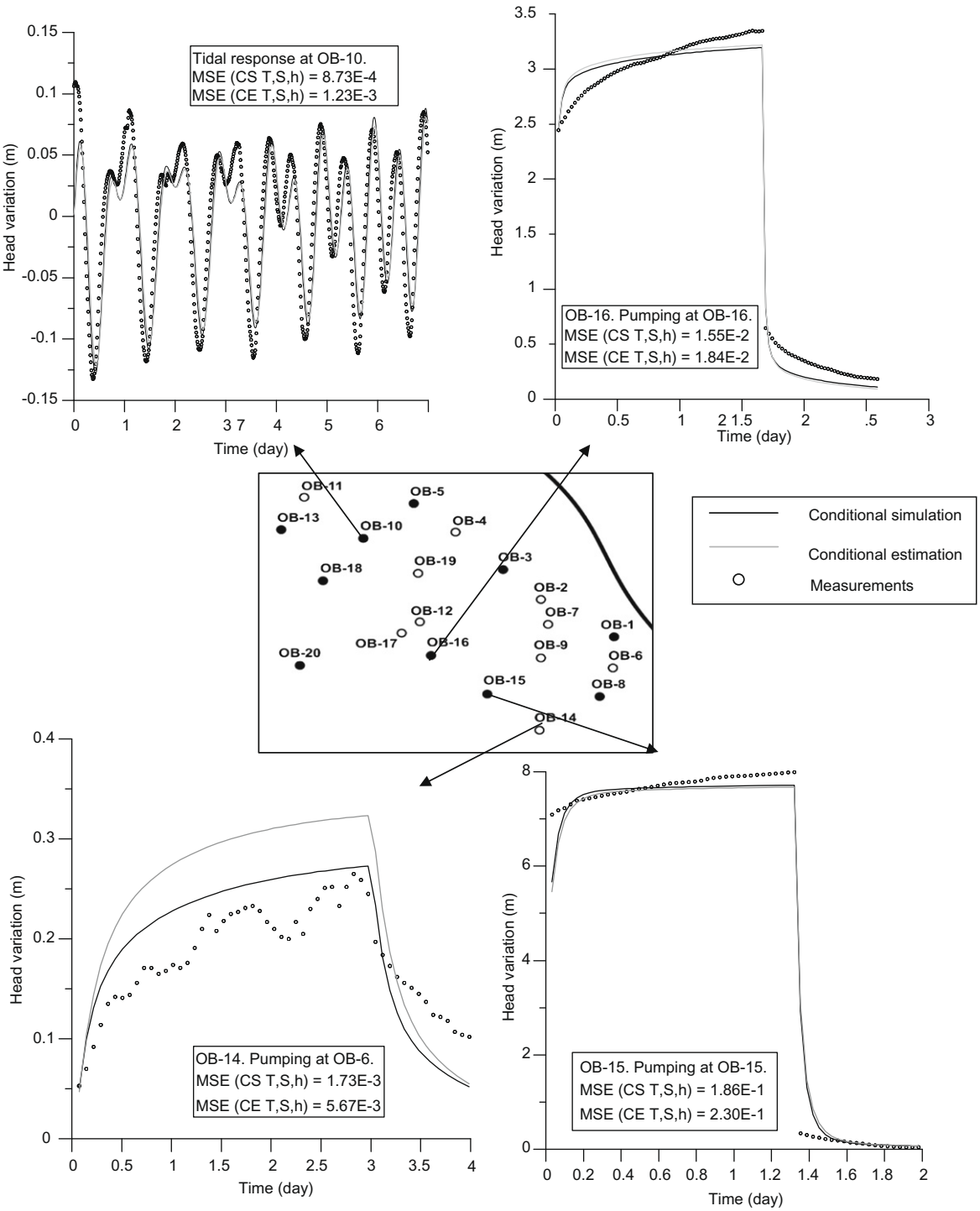

Fig. 7. Calculated and measured head variations at selected points in response to tidal and pumping effects. In the insets, MSE denotes mean square error (mean square difference between calculated and measured head variations). CS and CE denote conditional simulation and conditional estimation, respectively.

drawdown caused by pumping at wells OB6, OB15 and OB16 (1.22, 7.99 and 3.35 m, respectively). In addition, mean residuals obtained by conditional estimation are depicted. Three observations arise from Fig. 8. First, all boxplots are centered on a small value, regardless of the forcing term. Thus, the median of the residuals is small. This reflects the good quality of the fits for all the realizations. Second, mean residuals obtained by conditional estimation are, in general, slightly larger than those obtained by conditional simulation. However, these differences are not significant in any case. Third, the wings of the boxplots are short. This manifests the striking similarity between the simulated fields displayed in Figs. 5 and 6 (i.e., similar fits are obtained by different realizations). None of the simulations deviate significantly from the field obtained by conditional estimation. This convergence toward similar fields is even more striking when considering that the 200 initial simulations, conditioned only to T and S data (not depicted here) were all very different. After conditioning to head variations, they all became very similar. We argue that the information contained in the head variation measurements is sufficient to reduce uncertainty.

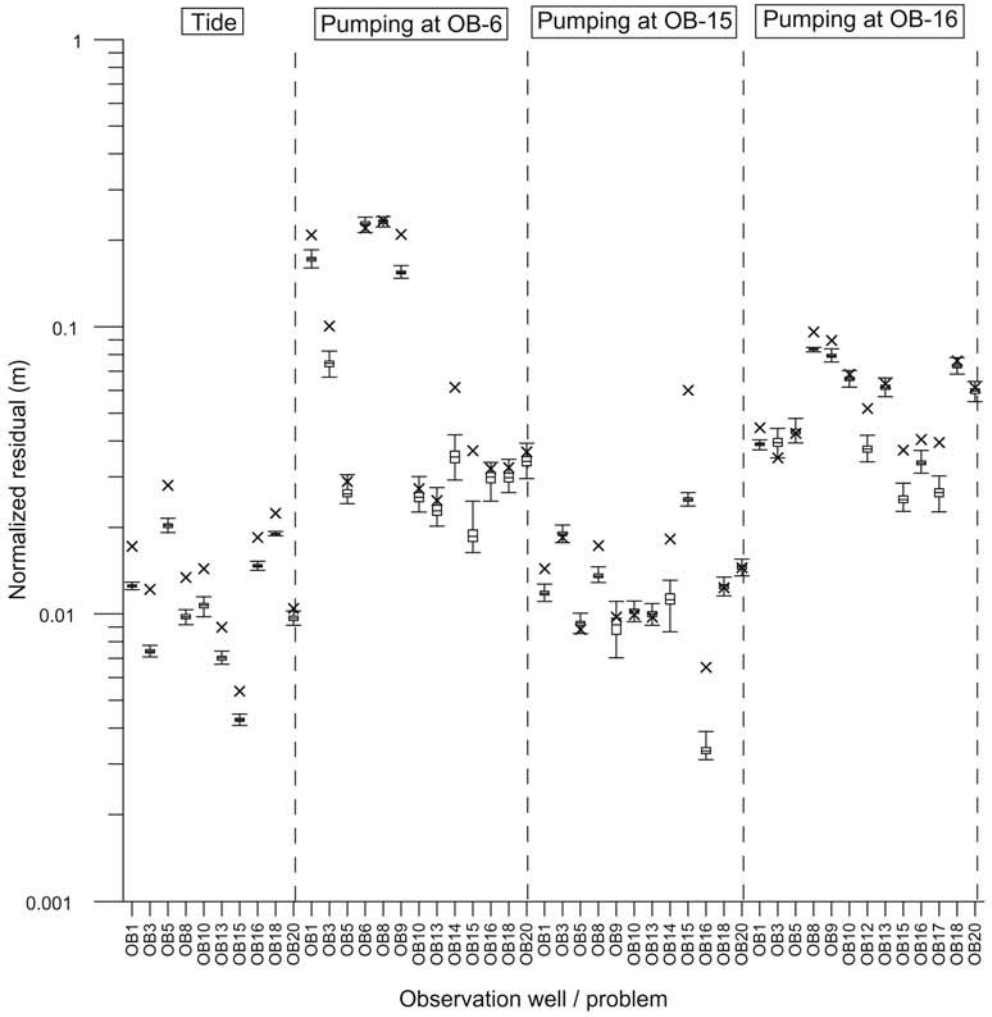

Fig. 8. Box and Whisker plots of standardized residuals (averaged in time). Normalization factors are the amplitude of the tide (2.62 m) and the maximum drawdown at the pumping well (1.22, 7.99 and 3.35 m for pumping at wells OB-6, OB-15 and OB-16, respectively). Crosses depict mean standardised residuals obtained by conditional estimation.

From a qualitative point of view, all transmissivity (and diffusivity) fields resemble vaguely the directional features of connectivity as observed in the resistivity map (Fig. 1). This comparison also reveals the presence of highly conductive bodies well connected to the sea in the resistivity map and all simulations. We further tested the physical plausibility of the simulated fields by comparing the values of effective diffusivity obtained by the TRM (see section "Analysis of the tidal response") with those obtained by the stochastic model (Table 2). It is worth mentioning that the former data set was not used as conditioning data for the geostatistical inversion. The fact that both the TRM and the geostatistical model yield similar values of effective diffusivity is a good indication of the physical plausibility of the simulations.

From the above we conclude that the available data sets and the techniques used for aquifer characterization are available to identify the main patterns of heterogeneity. The surprising finding was the limited degree of variability of the simulated fields. Yet, there is still room for uncertainty due to errors in the conceptual model

Table 4
Parameters required by the genetic algorithm used for the optimization of the pumping network.

Value			
C_{unit}	77,169 Euro/(m^4/s). Assuming 22 years of exploitation and an unitary cost of 0.0399 Euro/kWh.		
	Category	D (Euro/well)	D + P (Euro / well)
Drilling cost (D)/Cost of Pump (P)	360 m^3/h	23,650	224,327
	252 m^3/h	23,650	190,678
	108 m^3/h	0 (existing wells)	100,000
Number of potential wells		126	
Population at each generation		30	
Number of generations		250,000	
Maximum drawdown allowed		15 m	
Penalty factor for drawdowns		100	
Target discharge		10,000 m^3/h (security factor of 1.111)	
Penalty factor for discharge		1000	

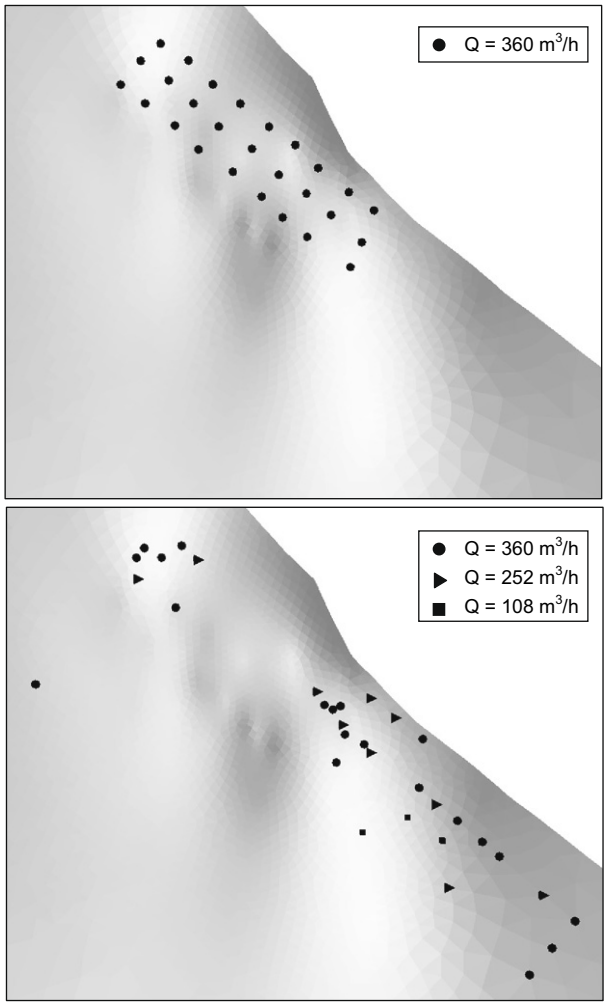

Fig. 9. Synthetic (above) and optimum (below) pumping networks. On the background, a shaded relief of the average diffusivity field (Fig. 6, on bottom).

that were not accounted for in this study (e.g., the choice of correlation structure defining the geostatistical model, the boundary conditions and the position of the seashore, etc.).

Optimum pumping network

The 200 equally likely hydraulic characterizations are used to find a unique optimally-robust design of the pumping network, defined by the number of wells, their location and the corresponding discharge rates. In this optimization framework, a robust design (Watkins and McKinney, 1997) is defined such that, first, it satisfies the design constraints for all the hydraulic characterizations generated at the previous step. Second, it minimizes the total expected costs of set up, operation and maintenance of the solution (mean over all the simulations). More precisely, constraints of the design are:

- A target discharge of 9000 m^3/h. In fact, the solution is slightly over-designed, in order to ensure the groundwater supply to the desalination plant, so as to warrant the required production of 3346 m^3/h of freshwater. This also accounts for potential stops at some wells for maintenance or repairing. Finally, the applied target discharge is 10,000 m^3/h.
- The solution must be technically feasible. Only three types of pump capable of handling highly aggressive brackish water with pumping rates of 360, 252 and 108 m^3/h are available.

The objective is then to minimize the impacts of pumping and the costs of drilling, maintenance and exploitation. This is partly achieved by minimizing drawdowns, which reduces impacts to the aquifer, electrical costs, risks of well collapse, etc.

Problem formulation and genetic algorithm

Under the aforementioned constraints, we solve a discrete (only three pumping rates can be considered), non linear (i.e., costs are not a linear function of pumping rates) optimization problem in a stochastic framework. Two techniques are applied. On the one hand, we used genetic algorithms to solve the aforementioned problem (Goldberg, 1989; Siegfried and Kinzelbach, 2006). On the other hand, a stacking approach (Wagner and Gorelick, 1987; Chan, 1993, 1994; Morgan et al., 1993; Feyen and Gorelick, 2004) accounts for the inherent stochastic uncertainty. In order to keep calculation times reasonable, 126 mesh nodes have been selected as potential locations for the wells. Nodes at existing wells (Fig. 1) are included in the set of potential well locations. These are located in the highly diffusive bodies (Fig. 6) and within the lot owned by the desalination company. The 126 unknowns are the type of pump at each potential well, ranging from 0 (no pump) to 3 (maximum flow rate of 360 m^3/h). These are arranged as a vector of integers $\mathbf{x}$, termed individual.

By virtue of the superposition principle, one can compute the drawdowns associated to a given individual $\mathbf{x}$ with the aid of a response matrix $\mathbf{A}$ (i.e., the element a_{ij} being the drawdown at well 'i' in response to a unitary pumping at potential well 'j'). The components of $\mathbf{A}$ are calculated by running the model for a given transmissivity field successively considering all potential locations for the pumping wells. A steady state regime with pumping was used to consider the worst case situation. Only 100 out of 200 transmissivity fields were considered for the optimization network, as increasing the stack size adds more constraints, which makes it more tedious to find a robust solution (Feyen and Gorelick, 2004). In fact, the stack size was reduced due to CPU considerations (an optimization run using 100 transmissivity fields already takes 24 h in a high performance computer). A stacked matrix $\mathbf{A}^{\text{stack}}$ (Feyen and Gorelick, 2004) accounts for the response matrices corresponding to the 100 transmissivity fields. Drawdowns can then be expressed as

$$\mathbf{s} = \mathbf{A}^{\text{stack}}\mathbf{Q}(\mathbf{x} \qquad 3)$$

where $\mathbf{s}$ is a vector containing the drawdowns at all potential wells and for all stochastic simulations due to the pumping configuration $\mathbf{x}$ and $\mathbf{Q}$ is a vector containing the flow rates associated to the categories defined by the individual $\mathbf{x}$. The use of $\mathbf{A}^{\text{stack}}$ warrants that the constraints are met for all considered transmissivity fields.

Given an individual $\mathbf{x}$ and its associated drawdowns, the cost function over all wells and all stochastic simulations can be defined as

$$C = \sum_{j=1}^{Nsimu} \sum_{i=1}^{Nwells} (D_i + P_i + E_{i,j} \qquad 4)$$

where '*Nwells*' and '*Nsimu*' denote the number of potential wells and stochastic simulations, respectively. D_i, P_i and $E_{i,j}$ are the drilling cost, the cost of the pump and its maintenance and the electrical costs at well 'i' and simulation 'j', respectively. Note that only the electrical costs depend on the simulation. Calculating D and P is straightforward, as they depend only on the category of the pump and the position (already existing wells have a drilling cost equal to zero). Electrical costs can be expressed in terms of potential energy of groundwater E_p:

$$Ep_i = mgh = (Q_i \rho t) g s_i \quad [\text{Joule} \qquad 5)$$

where Ep_i is the potential energy at well 'i', m is mass of water [kg], g is gravity [m/s^2], h is the required height of elevation [m], Q_i is the flow rate at well 'i' [m^3/s], ρ is density (1032 kg/m^3), t is time [s] and s_i [m] is the drawdown at well 'i'. Time is set to 22 years, the expected life of the desalination plant. Finally, grouping all constant terms, E_i is expressed as

$$E_i = Ep_i[\text{kWh}]\beta[\text{euro/kWh}] = Q_i s_i C_{unit} \quad (6)$$

where β denotes the unitary cost of electricity (0.0399 Euro/kWh) and C_{unit} is 77169 Euro/(m^4/s). Fixed costs and other parameters of the genetic algorithm are summarized in Table 4.

Posed in this way, the problem of minimizing the electrical costs E is equivalent to that of minimizing the drawdown at the pumping wells. Once the individual **x** has been designed, additional constraints due to target discharge and maximum allowed drawdown are addressed by multiplying the cost function by a penalty factor when these criteria are not met. Actually, the maximum drawdown allowed (15 m in this case) was not attained for any simulation in the stack.The optimum individual **x** is determined by the GaMin Matlab toolbox (see a detailed description in Popov, 2005). After performing a sensitivity analysis to study the convergence and the reliability of the solution, the size of the population has been set to 30 individuals. We used a conventional scattered cross-over mechanism. The mutation range and the part of the population copied to the next generation (elite coefficient) have been set to 20% and 7%, respectively. The part of the population with largest objective functions is replaced by new individuals (7%). Finally, the number of generations was set to 250,000.

Optimization results

The benefit of optimization is analyzed by comparing two pumping configurations. First, we test a tradition based, hand-delineated, pumping network arising from a preliminary study not accounting for optimization. In that solution, it was planned to locate 27 pumping wells along three lines parallel to the sea-

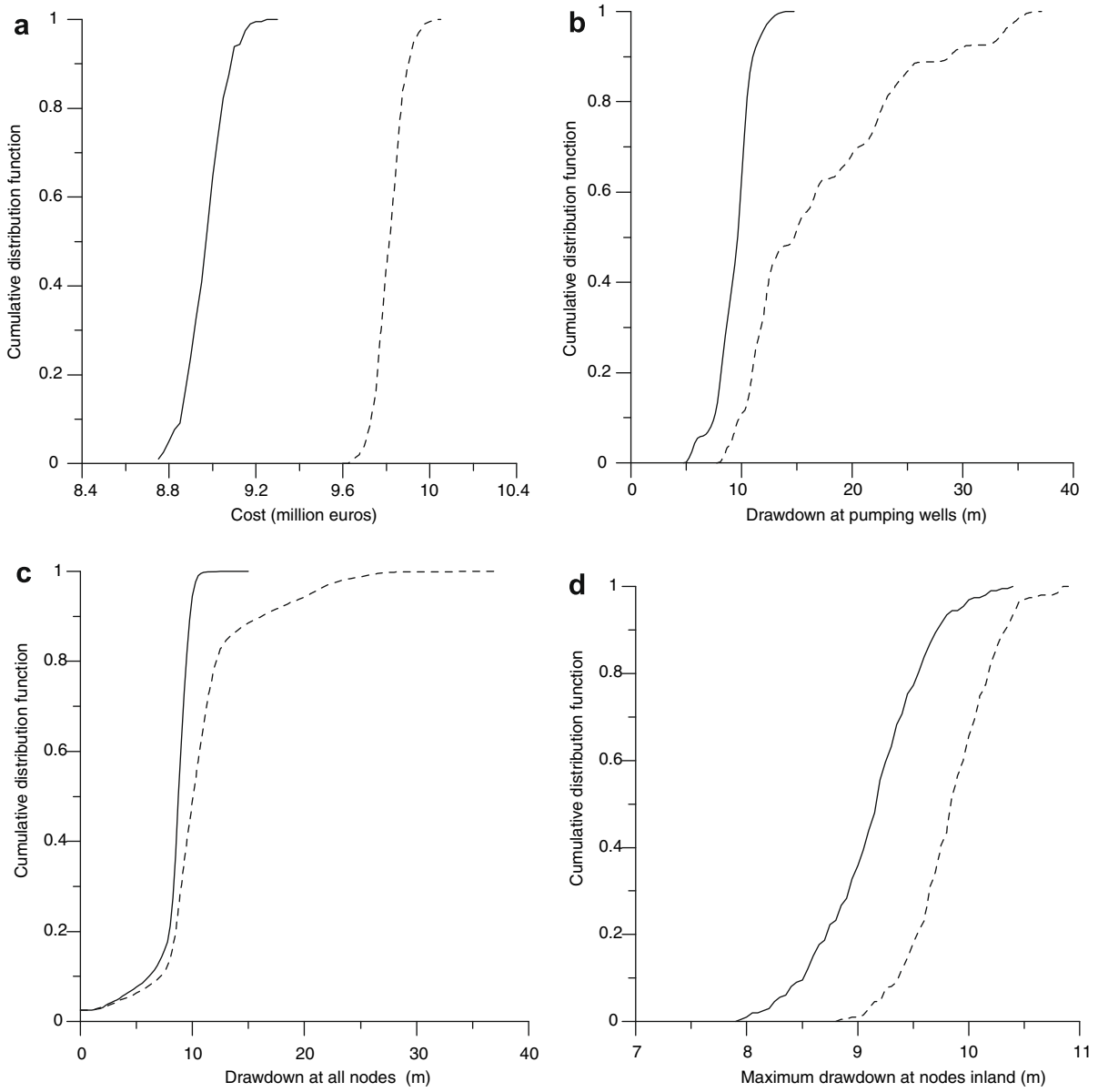

Fig. 10. Cumulative distribution functions of optimum (solid line) and synthetic (dashed line) pumping networks: (a) cost function, (b) drawdown at pumping wells, (c) drawdowns at all nodes of the finite element mesh and (d) drawdown at nodes defining the inland boundary of the model.

Table 5
Statistics of the comparison between the synthetic and the optimum pumping networks.

		Minimum	Maximum	Average	Standard deviation
Cost function (million euros)	Optimum	8.75	9.23	8.98	0.09
	Synthetic	9.65	10.0	9.82	0.06
Drawdown at pumping wells (m)	Optimum	4.76	14.65	9.47	1.57
	Synthetic	7.71	37.04	17.08	7.28
Drawdown at all nodes (m)	Optimum	0.00	14.65	8.36	2.03
	Synthetic	0.00	37.04	10.89	4.43
Maximum drawdown at nodes inland (m)	Optimum	7.93	10.38	9.15	0.48
	Synthetic	8.85	10.87	9.87	0.37

shore, following current practice. Pumping rate is identical at all wells (i.e., target discharge of 10000 m^3/h divided by the number of wells). Second, we optimize the pumping configuration for 100 transmissivity fields. Results are evaluated in terms of cost of the solution and drawdowns at the pumping wells, at all nodes of the finite element mesh and at those defining the inland boundary. Fig. 9 displays the synthetic and optimum pumping configurations. Fig. 10 displays the cumulative distribution functions (cdf hereinafter) of costs and drawdowns. Statistics of those cdfs are summarized in Table 5. It is worth emphasizing that the optimization was performed using 100 transmissivity fields. However, the performance of the optimum and synthetic networks is evaluated for the complete stack of 200 realizations. The optimum transmissivity field obtained by conditional estimation was not considered for optimization as it does not allow us to evaluate the uncertainty of the suggested solution.

The optimum distribution of wells (and corresponding flow rates) is reasonable, as observed in Fig. 9. In general, largest pumping rates of 360 m^3/h correspond to wells along the two high diffusivity channels. This causes little drawdowns and a superior yield of the system. Flow rates of 252 and 108 m^3/h are assigned mainly to existing wells. We attribute this to the fact that drilling costs are zero at existing wells.

The effect of the optimization is best analyzed observing Fig. 10 and Table 5. First, the total cost of the system is reduced substantially (Fig. 10a). In average, the reduction is of about 10% of the total cost. The underlying uncertainty is very small, as measured by the standard deviation of the cost function. Second, it reduces significantly the drawdowns (at the pumping wells, at all nodes and at those defining the inland boundary; Fig. 10 b, c and d, respectively). Thus, the optimum pumping configuration minimizes the total cost and the inherent environmental hazards. This effect is best observed in Table 5. On average, the optimum configuration reduces the drawdown at pumping wells by approximately 8 m. This minimizes both the risk of the pump failure and of well collapse. This reduction is not dramatic in terms of generalized drawdowns or drawdowns at nodes defining inland boundary (average reduction of 2.5 m and 0.75 m, respectively). These magnitudes are more sensitive to the amount of water being removed rather than to the location/configuration of the removal. A maximum drawdown of 10 m (30 m for the synthetic network) is barely achieved at a few transmissivity fields which were not considered for the optimization. This confirms that the optimum pumping network also accounts for minimum aquifer vulnerability.

Conclusions

This work summarizes the application of stochastic inverse modeling and optimization techniques to the management of a pumping system at a coastal aquifer in Oman. A stochastic characterization of hydraulic parameters from tidal fluctuation and pumping test data was used to design an optimum pumping network of brackish groundwater. This would allow an increase in the current production of a desalination plant, which will satisfy the growing demand of freshwater within the area.

The applied methodology consists of two main steps. First, transmissivity and storage coefficient fields are characterized from available data using a stochastic model. Spatial variability of these parameters is addressed by the regularized pilot points method. We obtain 200 equally likely simulations of the transmissivity and storage coefficient fields that are plausible (i.e., fit the diffusivities obtained by TRM and resemble the connectivity features of a resistivity map obtained by geophysics) and fit well the indirect head variation measurements.

Second, an optimum pumping network is designed with the help of a genetic algorithm. The aim is to obtain a reliable solution that minimizes the expected cost and that allocates the pumping wells in such a way that the drawdowns are small. This minimizes the electrical costs and the environmental side effects. Constraints of the design are the target discharge (10,000 m^3/h) and the technical feasibility of the solution (i.e., predefined pumping rates of 360, 252 and 108 m^3/h).

The performance of the optimum solution is compared to the one of a synthetic, tradition based, hand-delineated, pumping network. Results show that the use of the optimization technique leads to a reduction in operational costs of more than 10%. In addition, drawdowns are reduced dramatically. Certainly, this cannot be considered as a fair comparison, since different reduction factors could be obtained when comparing the optimum solution with other configurations, traditionally designed in a subjective way by water managers.

Much remains to be done. Uncertainties on the conceptual model were neglected in this work. Among them, the location of the contact between aquifer and sea may have a large impact on the calibration results. Geophysics and tracer tests can provide valuable information for the identification of the karstic conduits. These data sets could be considered as conditioning data for the stochastic model. Non multi-Gaussian techniques, such as multiple point geostatistics could be useful to infer patterns of heterogeneity in a more realistic manner. Yet, this work demonstrates the value of combining stochastic inverse modeling to infer aquifer heterogeneity and optimization techniques to determine (objectively) the optimum pumping configuration. This is a promising methodology for designing pumping networks in highly heterogeneous aquifers while also minimizing the environmental impacts of desalination plants.

Acknowledgments

Funding for this work was partly provided by the Swiss National Science Foundation (Contract PP002-106557). The authors wish to thank David Ginsbourger for his advice with regard to optimization techniques and J. Malcolm Ashworth for his outstanding field work. We also thank Harrie Jan Hendricks Franssen and an anonymous reviewer for their comments helping to improve the quality of the paper. We thank Nico Goldscheider, Luit Jan Slooten, Nicho-

las Wolfe and Nicholas Lombardi for early reviews of the manuscript.

References

Abarca, E., Vazquez-Sune, E., Carrera, J., Capino, B., Gamez, D., Batlle, F., 2006. Optimal design of measures to correct seawater intrusion. Water Resour. Res. 42 (9), W09415.

Ahlfeld, D.P., Heidari, M., 1994. Applications of optimal hydraulic control to groundwater systems. J. Water Resour. Plan. Manage. 120 (3), 350–365.

Ahlfeld, D.P., Mulligan, A.E., 2000. Optimal Management of Flow in Groundwater Systems. Academic Press, San Diego. 185pp.

Alcolea, A., Carrera, J., Medina, A., 2006a. Inversion of heterogeneous parabolic-type equations using the pilot points method. Int. J. Numer. Methods Fl. 51 (9–10), 963–980.

Alcolea, A., Carrera, J., Medina, A., 2006b. Pilot points method incorporating prior information for solving the groundwater flow inverse problem. Adv. Water Res. 29, 1678–1689.

Alcolea, A., Carrera, J., Medina, A., 2008. Regularized pilot points method for reproducing the effect of small scale variability. Application to simulations of contaminant transport. J. Hydrol. 355 (1–4), 76–90.

Alcolea, A., Castro, E., Barbieri, M., Carrera, J., Bea, S.A., 2007. Inverse modeling of coastal aquifers using tidal response and hydraulic tests. Ground Water 45 (6), 711–722.

Bugeda, G., 1990. Utilización De Técnicas De Estimación De Error Y Generación Automática De Mallas En Procesos De Optimización Estructural. Technical University of Catalonia, Barcelona.

Carrera, J., Neuman, S.P., 1986a. Estimation of aquifer parameters under transient and steady-state conditions, 2. Uniqueness, stability and solution algorithms. Water Resour. Res. 22 (2), 211–227.

Carrera, J., Neuman, S.P., 1986b. Estimation of aquifer parameters under transient and steady-state conditions, 3. Applications. Water Resour. Res. 22 (2), 228–242.

Chan, N., 1993. Robustness if the multiple realization method for stochastic hydraulic aquifer management. Water Resour. Res. 29 (9), 3159–3167.

Chan, N., 1994. Partial infeasibility method for change-constrained aquifer management. J. Water Resour. Plan. Manage. 120 (1), 70–89.

Chen, C., Jiao, J.J., 1999. Numerical simulation of pumping tests in multilayer wells with non-Darcian flow in the well-bore. Ground Water 37 (3), 465–474.

Cheng, A.H.D., Halhal, D., Naji, A., Ouazar, D., 2000. Pumping optimization in saltwater-intruded coastal aquifers. Water Resour. Res. 36 (8), 2155–2165.

Cornaton, F., 2007. A 3-D Ground water flow and transport finite element simulator, Neuchatel. Ground Water.

Delyannis, E., 2003. Historic background of desalination and renewable energies. Sol. Energy 75, 357–366.

Dickie, P., 2007. Desalination: option for distraction for a thirsty world? WWF Global Freshwater Programme.

Ferris, J.G., 1951. Cyclic fluctuations of water level as basis for determining aquifer transmissibility. In: International Association of Hydrological Sciences, Publication 33, vol. 2. IAHS, Wallingford, UK, pp. 148–155.

Feyen, L., Gorelick, S.M., 2004. Reliable groundwater management in hydroecologically sensitive areas. Water Resour. Res. 40 (7).

Goldberg, D.E., 1989. Genetic Algorithms in Search, Optimization, and Machine Learning. Addison-Wesley, Berlin. 412pp.

Gorelick, G., 1983. A review of distributed parameter groundwater modeling methods. Water Resour. Res. 19 (2), 305–319.

GWI, 2005. 19th IDA Worldwide Desalting Plant Inventory. Media Analytics Limited (Global Water Intelligence), Oxford, UK.

GWI, 2006. Desalination Markets 2007: A Global Industry Forecast. Media Analytics Limited (Global Water Intelligence). Oxford, UK.

Hendricks Franssen, H.J., Gomez-Hernandez, J.J., Sahuquillo, A., Capilla, J.E., 1999. Joint simulation of transmissivity and storativity fields conditional to hydraulic head data. Adv. Water Resour. 23, 1–13.

Hvorslev M.J., 1951. Time-lag and soil permeability in ground-water observations. Bulletin 36. Vicksburg, Mississippi. US Army Corps of Engineers, Waterways Experiment Station.

Li, W., Englert, A., Cirpka, O.A., Vanderborght, J., Vereecken, H., 2007. Two-dimensional characterization of hydraulic heterogeneity by multiple pumping tests. Water Resour. Res. 43 (4), W04433.

Mantoglou, A., 2003. Pumping management of coastal aquifers using analytical models of saltwater intrusion. Water Resour. Res. 39 (12).

Medina, A., Alcolea, A., Carrera, J., Castro, L.F., 2000. Modelos de flujo y transporte en la geosfera: Codigo Transin IV. [Flow and transport modelling in the geosphere: the code TRANSIN IV]. IV Jornadas de Investigacion y Desarrollo Tecnologico de Gestion de Residuos Radiactivos de ENRESA. ENRESA, Barcelona, pp. 195–200.

Medina, A., Carrera, J., 2003. Geostatistical inversion of coupled problems: dealing with computational burden and different types of data. J. Hydrol. 281, 251–264.

Meier, P., Carrera, J., Sanchez-Vila, X., 1998. An evaluation of Jacob's method work for the interpretation of pumping tests in heterogeneous formations. Water Resour. Res. 34 (5), 1011–1025.

Morgan, D.R., Eheart, J.W., Vallocchi, A.J., 1993. Aquifer remediation design under uncertainty using a new chance constrained programming technique. Water Resour. Res. 29 (3), 551–561.

Popov, A., Filipova, K., 2004. Genetic algorithms – synthesis of finite state machines. In: Proceedings of the 27th Spring Seminar on Electronics Technology, pp. 388–392.

Popov, A., 2005. Genetic Algorithms for optimization, User Manual, Hamburg.

Renard, P., 2007a. HYTOOL c1.91. User's guide, Neuchatel.

Renard, P., 2007b. Stochastic hydrogeology: what professionals really need? Ground Water 45 (5), 531–541.

Rotting, T., Carrera, J., Bolzicco, J., Salvany, J.M., 2006. Stream-stage response tests and their joint interpretation with pumping tests. Ground Water 44 (3), 371–385.

Siegfried, T., Kinzelbach, W., 2006. A multiobjective distre stochastic optimization approach to shared aquifer management: methodology and application. Water Resour. Res. 42 (W02402). doi:10.1029/2005WR004321.

Tarantola, A., 2005. Inverse Problem Theory and Methods for Parameter Estimation. SIAM, 342pp.

Tarantola, A., 2006. Popper, Bayes and the inverse problem. Nature Phys. 2, 492–494.

Trefry, M.G., Johnston, C.D., 1998. Pumping test analysis for a tidally forced aquifer. Ground Water 36 (3), 427–433.

Wagner, B., Gorelick, S.M., 1987. Optimal groundwater quality management under parameter uncertainty. Water Resour. Res. 23 (7), 1162–1174.

Wagner, B., 1995. Recent advances in simulation optimization groundwater management modeling. Rev. Geophys. 33, 1021–1028.

Watkins Jr, D.W., McKinney, D.C., 1997. Finding robust solutions to water resources problems. J. Water Resour. Plan. Manage, ASCE 123 (1), 49–58.

Weiss, R., Smith, L., 1998. Parameter space methods in joint parameter estimation for groundwater flow models. Water Resour. Res. 34 (4), 647–661.